Ion-Atom Potential Energy Functions Obtained from kev Scattering Data*

G. H. LANE† AND E. EVERHART
Physics Department, University of Connecticut, Storrs, Connecticut
(Received August 15, 1960)

The potential energy functions between ions and atoms in collision are determined from experimental data. The ion-atom combinations studied include Ar^+ on Ar, Ne^+ on Ar, Ne^+ on Ne, He^+ on Ar, He^+ on Ne, and He^+ on He, using differential cross-section measurements by Fuls *et al.* and Jones *et al.* made at 25, 50, and 100 kev. These data are analyzed using equations developed by Firsov. The potential energies are positive, are in the range of one to sixty thousand electron volts, and correspond to ion-atom separations of a small fraction of an angstrom.

The resultant potential energy curves are compared with a function derived by Firsov from a statistical model and they are found to fit fairly well. The fit to an exponentially screened Coulomb potential energy curve is not quite as good, but both these theoretical curves fall within the accuracy of the experimental data.

1. INTRODUCTION

THE potential energy function between ions and atoms in kilovolt energy collisions is of interest because it determines their scattering. The repulsive Coulomb force between the nuclei is modified by a factor which is due to the electron screening. Several functions have been proposed for this potential energy, including an exponentially screened Coulomb function[1] and a function derived by Firsov[2] from a statistical model based on the Thomas-Fermi calculation.

The potential energy function can be determined from experimental data in several ways:

(1) Measured values of the differential cross section can be compared directly with values calculated from arbitrarily assumed potential energy functions. Thus Fuls *et al.*[3] compared their experimental differential cross section data for noble gas ion-atom collisions with the calculation of Everhart *et al.*[4] who assumed an exponentially screened Coulomb potential energy function. The agreement was fairly good, though not exact.

(2) The impact parameter can be determined at selected angles and at several energies using methods developed by Amdur[5] and Simons.[6] A power-law potential energy is assumed and the corresponding calculated impact parameter dependence is fitted to the data. Mason and Vanderslice[7] have calculated improved potential energy functions for use with this method. The energy range of Amdur and Simons experimental work is 4 ev to 2000 ev and therefore corresponds to larger interatomic separations than the work which is reported below.

(3) In the present paper a new method is used which is the inverse of method (1). The scattering data is used to determine the potential energy function uniquely. The first step is to use differential cross section data to find the angular dependence of the impact parameter. The second step is to find, from this, the potential energy as a function of separation distance. This second step is by far the more difficult. Formulas developed by Hoyt[8] required using data taken at several energies to determine the desired potential energy function. Firsov[9] developed a much improved procedure which determines the potential energy function uniquely from data taken at one incident energy. Firsov's method is here applied for the first time to experimental data.

The recent experiments by Fuls *et al.*,[3] Jones *et al.*,[10] and Kaminker and Fedorenko[11] have accumulated absolute data on the differential scattering of ions and atoms which this method requires. Potential energies of Ar^+ ions incident on Ar atoms, Ne^+ on Ar and Ne, and He^+ on Ar, Ne, and He are determined here from data taken at 25, 50, and 100 kev (laboratory) incident energies.

2. THEORY

The differential cross section $\sigma(\theta)$ and scattering angle θ, both in center-of-mass coordinates, are easily obtained by transforming the experimental values $\sigma(\Theta)$ and Θ, which are in the laboratory system. The impact

* This work was sponsored by the Office of Ordnance Research, U. S. Army, through the Ordnance Material Research Office at Watertown and the Boston Ordnance District.

† Now at Norwich University, Northfield, Vermont.

[1] N. Bohr, Kgl. Danske Videnskab. Selskab, Mat.-fys. Medd. **18**, 8 (1948).

[2] O. B. Firsov, J. Exptl. Theoret. Phys. (U.S.S.R.) **33**, 696 (1957) [translation: Soviet Phys.-JETP **6**, 534 (1958)].

[3] E. N. Fuls, P. R. Jones, F. P. Ziemba, and E. Everhart, Phys. Rev. **107**, 704 (1957).

[4] E. Everhart, G. Stone, and R. J. Carbone, Phys. Rev. **99**, 1287 (1955).

[5] I. Amdur and E. A. Mason, J. Chem. Phys. **25**, 624 (1956) and previous papers.

[6] W. H. Cramer and J. H. Simons, J. Chem. Phys. **26**, 1272 (1957) and previous papers.

[7] E. A. Mason and J. T. Vanderslice, J. Chem. Phys. **29**, 361 (1958) and previous papers.

[8] F. C. Hoyt, Phys. Rev. **55**, 664 (1939).

[9] O. B. Firsov, J. Exptl. Theoret. Phys. (U.S.S.R.) **24**, 279 (1953).

[10] P. R. Jones, F. P. Ziemba, H. A. Moses, and E. Everhart, Phys. Rev. **113**, 182 (1959).

[11] D. M. Kaminker and N. V. Fedorenko, J. Tech. Phys. (U.S.S.R.) **25**, 2239 (1955). See also N. V. Fedorenko, L. G. Filippenko and I. P. Flaks, J. Tech. Phys. (U.S.S.R.) **30**, 49 (1960) [translation: Soviet Phys.-Tech. Phys. **5**, 45 (1960)].

parameter p is related to $\sigma(\theta)$ and θ by

$$2\pi\sigma(\theta)\sin\theta d\theta = -2\pi p dp, \tag{1}$$

and this is integrated to give

$$p^2 = 2\int_\theta^\pi \sigma(\theta)\sin\theta d\theta. \tag{2}$$

From classical scattering theory,[12] which is valid[1,4] for the present problem, the angle θ is related to the impact parameter p and the interaction potential energy function $V(r)$ through the equation

$$\theta = \pi - \int_{r_0}^\infty 2(p/r)[(1-V(r)/E)r^2 - p^2]^{-\frac{1}{2}}dr, \tag{3}$$

where E is the incident kinetic energy in the center-of-mass system and r_0 is the distance of closest approach. The integrand is infinite at $r=r_0$. This integration cannot be carried out directly since the unknown quantity $V(r)$ is in the integrand.

The next steps, leading to Eq. (10) below, follow Firsov,[9] and are reproduced briefly here because his paper is not available in translation. Let

$$\psi = [1-V(r)/E]r^2, \tag{4}$$

and Eq. (3) becomes

$$\theta = \pi - \int_{p^2}^\infty 2p(d\ln r/d\psi)(\psi-p^2)^{-\frac{1}{2}}d\psi, \tag{5}$$

where p^2 is the value of ψ at $r=r_0$. Since

$$\int_{p^2}^\infty p(d\ln\psi/d\psi)(\psi-p^2)^{-\frac{1}{2}}d\psi = \pi, \tag{6}$$

it is possible to rearrange Eq. (5) in the form

$$\theta(p) = \int_{p^2}^\infty p[d\ln(\psi_1/r^2)/d\psi_1](\psi_1-p^2)^{-\frac{1}{2}}d\psi_1. \tag{7}$$

The symbol ψ_1 is used here instead of ψ in order to distinguish it from ψ which appears in a limit of integration in the next equation. Equation (7) is multiplied by $dp/(p^2-\psi)^{\frac{1}{2}}$ and integrated over p from $\sqrt{\psi}$ to ∞:

$$\int_{\sqrt{\psi}}^\infty \frac{\theta(p)dp}{(p^2-\psi)^{\frac{1}{2}}} = \int_{\sqrt{\psi}}^\infty pdp\int_{p^2}^\infty \frac{[d\ln(\psi_1/r^2)/d\psi_1]d\psi_1}{(p^2-\psi)^{\frac{1}{2}}(\psi_1-p^2)^{\frac{1}{2}}}. \tag{8}$$

The integral on the right is transformed[13] and written as

$$\int_{\sqrt{\psi}}^\infty \frac{\theta(p)dp}{(p^2-\psi)^{\frac{1}{2}}} = \frac{1}{2}\int_\psi^\infty [d\ln(\psi_1/r^2)/d\psi_1]d\psi_1 \times \int_\psi^{\psi_1} \frac{d(p^2)}{(p^2-\psi)^{\frac{1}{2}}(\psi_1-p^2)^{\frac{1}{2}}} = (\pi/2)\ln(r^2/\psi). \tag{9}$$

When this is solved for r, Firsov's result

$$r(\psi) = \sqrt{\psi}\exp\left[(1/\pi)\int_{\sqrt{\psi}}^\infty \theta(p)(p^2-\psi)^{-\frac{1}{2}}dp\right] \tag{10}$$

is obtained. Knowing $r(\psi)$ and using Eq. (4) it is possible to determine $V(r)$. Firsov checked this method showing that it leads analytically to the Coulomb potential energy function when the well-known Rutherford differential cross section was used for $\sigma(\theta)$. Using our procedure, as outlined below, we also checked Firsov's equations by inserting numerical values of differential cross section from reference (4) showing that it leads back to the corresponding screened Coulomb potential energy function.

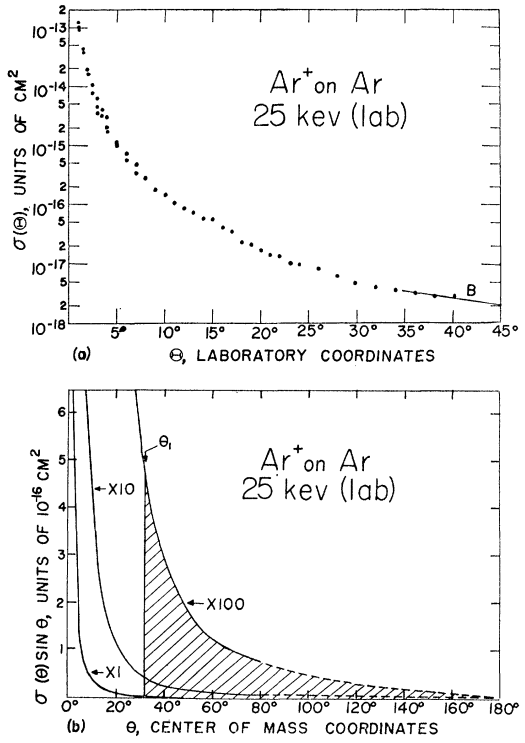

FIG. 1. (a) Differential cross-section data in laboratory coordinates for 25 kev Ar^+ on Ar collisions; (b) The above data is plotted in center-of-mass coordinates, weighting each cross section by the sine of the angle. The shaded area to the right of any particular angle θ_1 equals half the square of the corresponding impact parameter.

3. PROCEDURE

As an example of the procedure, let us consider the case of Ar^+ on Ar at 25 kev. Figure 1(a) shows the

[12] See, for example, H. S. W. Massey and E. H. S. Burhop, *Electronic and Ionic Impact Phenomena* (Oxford University Press, New York, 1952), p. 373.

[13] E. T. Whittaker and G. N. Watson, *Modern Analysis* (Cambridge University Press, Cambridge, 1927), 4th ed. See corollary in Sec. 4.51, p. 77.

differential cross section vs scattering angle in laboratory coordinates taken from Fig. 15 of reference (3) and Fig. 7(d) of reference (10). The solid lines in Fig. 1(b) show this same data transferred to center-of-mass coordinates[14] and weighted by the factor $\sin\theta$.

a. Determination of Impact Parameter

Numerical integration of the curve in Fig. 1(b) must be carried out as indicated in Eq. (2). This integral has an upper limit of 180° and thus it is necessary to make a reasonable extension of the data to 180° as indicated in the dotted line. The shaded area to the right of any particular angle θ_1, equals $p^2/2$. A portion of this area lies under the dotted line beyond the solid curve obtained from the data. When θ_1 is a small angle, this uncertain area is very small as seen in the ×1 and ×10 curves, and the determination of p is correspondingly accurate. However, when θ_1 is a moderately large angle, as in the case shown, the uncertain area can become an important fraction of the total. The effects of drawing the dotted extrapolation of Fig. 1(b) in various ways are considered in the appendix, Sec. 6(b), below.

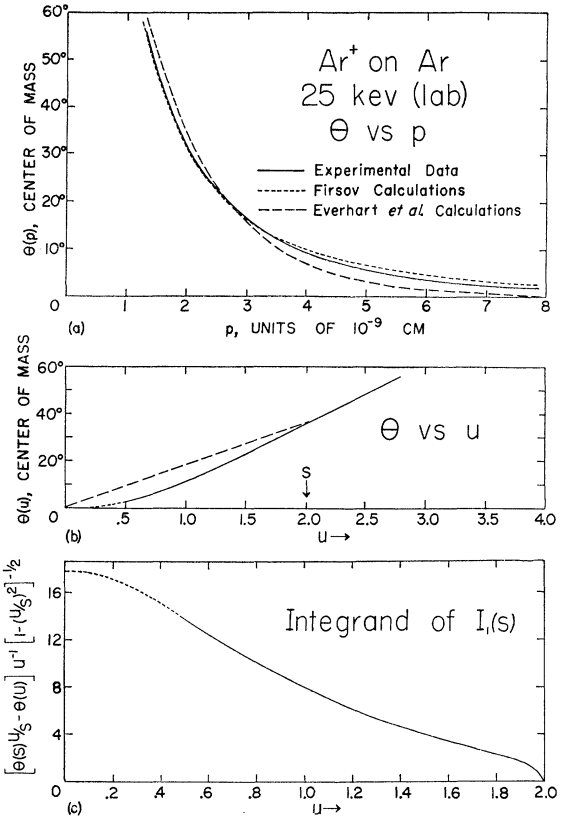

FIG. 2. (a) Scattering angle vs impact parameter is plotted from 25-kev Ar^+ on Ar data (solid line), from a calculation by Firsov (dotted line), and from a calculation by Everhart *et al.* (dashed line); (b) Scattering angle θ is plotted vs u which is a dimensionless reciprocal of the impact parameter (solid line). The dashed straight line is drawn to $\theta(s)$ where s is a particular value of u; (c) The integrand of $I_1(s)$ in Eq. (13) is plotted vs u.

The result of this integration is shown as the solid line of Fig. 2(a) which plots θ vs p. Although this is an intermediate result, it is interesting to compare now with a calculation by Firsov[15] (dotted line) and also with a calculation by Everhart *et al.*[4] (dashed line). These calculations use, respectively, the functions $V_f(r)$ and $V_b(r)$ to be described in Sec. 4 below.

b. Determination of $V(r)$

The next integration of the experimental curves is essentially that of Eq. (10). However, the infinities in the limit of integration and in the integrand of that equation require that its form be changed and adapted to numerical integration.

New dimensionless quantities

$$u=b/p \quad \text{and} \quad s=b/\sqrt{\psi} \tag{11}$$

are introduced, where the length b equals $Z_1Z_2e^2/E$. Here Z_1e and Z_2e are the nuclear charges of the colliding ion and atom. These are incorporated into Eq. (10) which now becomes

$$r/b=(1/s)\exp[I(s)/\pi],$$

where

$$I(s)=\int_0^s(\theta(u)/u)(1-u^2/s^2)^{-\frac{1}{2}}du. \tag{12}$$

The infinities in the integrand of $I(s)$ in Eq. (12) are avoided by rewriting it in the form,

$$I(s)=\int_0^s\frac{\theta(s)(u/s)du}{u(1-u^2/s^2)^{\frac{1}{2}}}-\int_0^s\frac{[\theta(s)(u/s)-\theta(u)]du}{u(1-u^2/s^2)^{\frac{1}{2}}}$$
$$=\theta(s)\pi/2-I_1(s). \tag{13}$$

Carrying through with the 25-kev Ar^+ on Ar example, the next step is to plot θ vs u as in the heavy solid line of Fig. 2(b). This is easily done from the curve of Fig. 2(a), since u is a dimensionless reciprocal of p. It is necessary to extend this line arbitrarily to $u=0$ as indicated by the dotted line in Fig. 2(b). This gap corresponds to the absence of experimental differential cross section data between 0° and 1° (lab). This is discussed in the appendix, Sec. 6(b), and it turns out that the final $rV(r)$ curves to be obtained are not very sensitive to the particular way this dotted line is drawn. A particular value of u, such as s, is chosen and the straight line $\theta(s)(u/s)$ is drawn as shown by the dashed line in Fig. 2(b). The difference between this line and the curve is the numerator of the integrand of $I_1(s)$.

The entire integrand of $I_1(s)$ (for the particular value of s chosen) is shown in Fig. 2(c). Near $u=0$ the

[14] See for example, L. I. Schiff, *Quantum Mechanics* (McGraw-Hill Book Company, Inc., New York, 1949), p. 99.

[15] O. B. Firsov, J. Exptl. Theoret. Phys. (U.S.S.R.) **34**, 447 (1958) [translation: Soviet Phys.-JETP **7**, 308 (1958)].

quantity $\theta(u)$ approaches zero and is much less than $\theta(s)(u/s)$ which also approaches zero. The integrand of $I_1(s)$ in Eq. (13) equals $\theta(s)/s$ at $u=0$. At the upper limit the integrand is zero. A curve similar to that of Fig. 2(c) is integrated numerically for each of several values of s. The resulting values of $I_1(s)$ are substituted into Eqs. (13) and (12) to find r/b for each value of s.

Corresponding values of r/b and s are then substituted into

$$V(r)=E[1-(1/s)^2(b/r)^2], \tag{14}$$

which is derived by combining Eqs. (4) and (11). As a result V is obtained as a function of r.

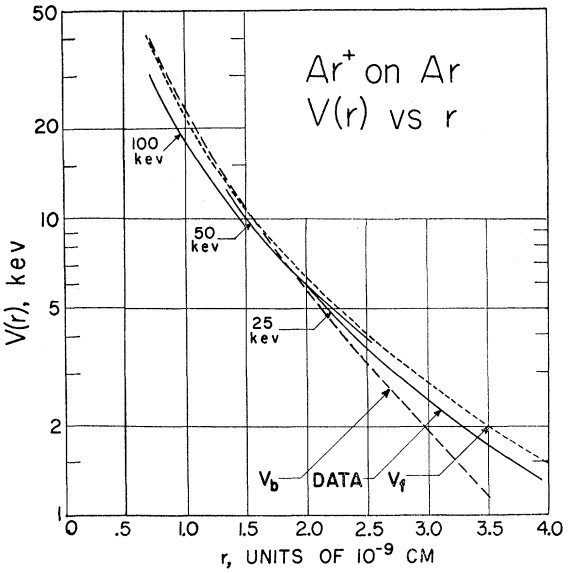

FIG. 3. The potential energy $V(r)$ is plotted as a function of the separation between an Ar^+ ion and an Ar atom. The three solid lines are calculated from experimental data taken at 100, 50, and 25-kev incident kinetic energies. The dotted line is a potential energy function derived by Firsov based on the Thomas-Fermi statistical model, and the dashed line is an exponentially screened Coulomb potential energy function.

4. RESULTS

Analyzing the data of Fuls *et al.*[3] and Jones *et al.*[10] as described above yields the potential energy curves shown in Fig. 3 for the Ar^+ on Ar case. The three solid lines, from left to right, correspond, respectively, to data taken at 100, 50, and 25 kev (lab). The dotted line corresponds to the function $V_f(r)$ obtained by Firsov.[2] He found that, to an accuracy of 10%, the interaction potential energy for ion-atom collisions calculated on the basis of the statistical model for the electrons can be represented as

$$V_f(r)=(Z_1Z_2e^2/r)\chi(x), \tag{15}$$

where $\chi(x)$ is the screening function in the Thomas-Fermi potential,[16] with $x=[Z_1^{\frac{1}{2}}+Z_2^{\frac{1}{2}}]^{\frac{2}{3}}(r/a_1)$ and $a_1=4.7\times10^{-9}$ cm. The dashed line in Fig. 3 is the screened Coulomb potential function, $V_b(r)$, given by

$$V_b(r)=(Z_1Z_2e^2/r)\exp(-r/a), \tag{16}$$

where $a=a_0/[Z_1^{\frac{2}{3}}+Z_2^{\frac{2}{3}}]^{\frac{1}{2}}$ as suggested by Bohr,[1] and $a_0=5.3\times10^{-9}$ cm. Both functions $V_f(r)$ and $V_b(r)$ fit the Ar^+ on Ar data curves fairly well, but in this representation all curves are so steep that it is difficult to analyze the differences.

The leading factor in both these potential energy functions is the same $1/r$ Coulomb term, but each has a different factor representing electron screening. Thus if one plots $rV(r)$ vs r there is a dual advantage: Firstly $rV(r)$ is proportional to the screening factor, which is of primary interest, and secondly, the curves are less precipitous and can be plotted on a better vertical scale.

Figure 4 shows plots of $rV(r)$ vs r obtained from the data for collisions of Ar^+ on Ar, Ne^+ on Ar, and Ne^+ on Ne. Figure 5 shows similar plots for He^+ on Ar, He^+ on Ne, and He^+ on He. Note that the horizontal scales are different in the several cases. On each figure

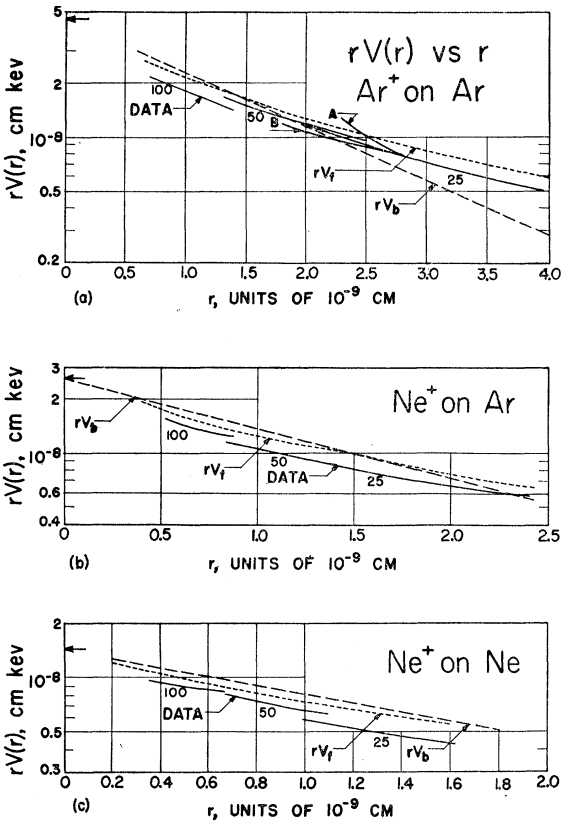

FIG. 4. Scattering data for (a) Ar^+ on Ar, (b) Ne^+ on Ar, and (c) Ne^+ on Ne taken at 100, 50, and 25 kev (lab). The product of the potential energy $V(r)$ and the separation r is plotted vs r. This product, $rV(r)$, which is proportional to the electron screening factor, is shown (solid lines) as determined from experimental data. For comparison $rV(r)$ is also shown for the Firsov potential energy function (dotted) and for the exponentially screened Coulomb potential energy function (dashed).

[16] V. Bush and S. H. Caldwell, Phys. Rev. 38, 1898 (1931).

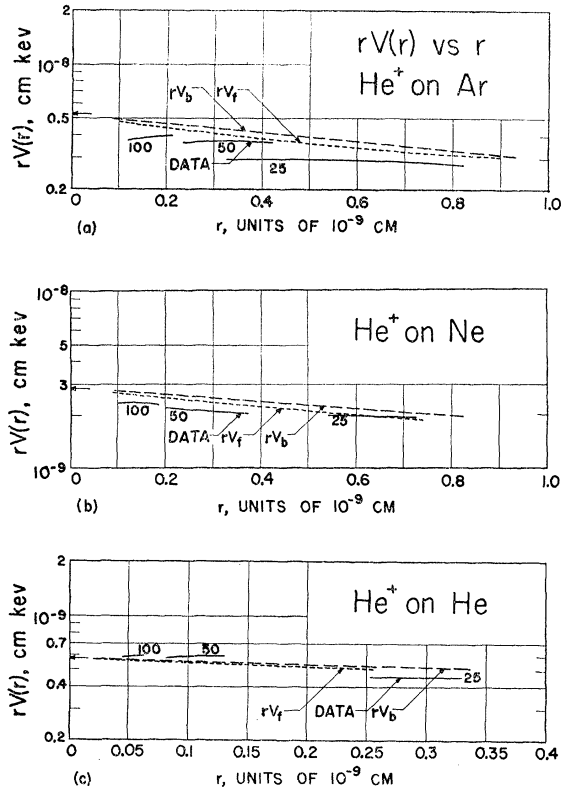

FIG. 5. Scattering data for (a) He^+ on Ar, (b) He^+ on Ne, and (c) He^+ on He taken at 100, 50, and 25 kev (lab). The product of the potential energy $V(r)$ and the separation r is plotted vs r. This product, $rV(r)$, which is proportional to the electron screening factor, is shown (solid lines) as determined from experimental data. For comparison $rV(r)$ is also shown for the Firsov potential energy function (dotted) and for the exponentially screened Coulomb potential energy function (dashed).

there is a separate solid line for data taken at each energy.

For some ion-atom combinations the three solid curves line up fairly well with each other, and for other combinations there are discontinuities. Two possible theoretical reasons for discontinuities in the curves are discussed:

(1) The potential energy may be velocity dependent to some extent. In this energy range the velocity of the incident ion is comparable to the velocity of the outer electrons of either atom. The electrons have more time to adjust themselves quasi-adiabatically in the 25-kev collisions than they do, for example, in the 50-kev collisions. The potential energy may be different in these two cases at the same interatomic distance.

(2) The classical theory used here in obtaining $V(r)$ from $\sigma(\theta)$ assumes elastic collisions, and is valid to the extent that the inelastic energy transferred in the collision process is very small compared to the incident kinetic energy. Such inelastic effects might cause discontinuities between curves taken at different energies.

However, it is probable that experimental error in the original data is sufficient in itself to cause discontinuities which mask either of the above considerations. The effects of systematic experimental errors and also the effects of extrapolations in the calculation procedure used here are discussed more fully in the appendix.

If there were no electron screening $rV(r)$ would equal $Z_1Z_2e^2$ as required by Coulomb's law. The data would then follow a horizontal line at this level, which is indicated by a small arrow on the ordinate for each combination. Thus, at each separation r, the measured value of the electron screening factor is found by taking the ratio of the corresponding value of $rV(r)$ to $Z_1Z_2e^2$.

For each case in Figs. 4 and 5 the screening factor χ of Eq. (15) is shown dotted and the screening factor $\exp(-r/a)$ of Eq. (16) is shown as a dashed straight line. These factors are weighted, of course, by $Z_1Z_2e^2$ for each combination in order to compare them with the data.

The screening factor χ has the same general curvature as the data curves of Figs. 4(a) and 4(b) and generally fits the data somewhat better then the exponential screening factor.

However, the potential energy functions of Eqs. (15) and (16) are both considered to fit the data well enough so that either may be used to calculate the forces between ions and atoms in the energy range studied here.

ACKNOWLEDGMENTS

We wish to thank Dr. Arnold Russek and Dr. Francis P. Ziemba for valuable discussions.

APPENDIX

Here the effects of experimental error and the effects of various extrapolation procedures of Sec. 3 are considered.

a. Experimental Errors

Reference to the experiments of Fuls *et al.*[3] and Jones *et al.*[10] shows that there are two important kinds of errors. The first of these is a "scale factor" error in determining absolute differential cross sections. Thus errors in measuring target gas pressure, incident ion beam energy, detector sensitivity, and solid angle dimensions will affect all data points taken during a given data run by the same factor. The importance of this scale factor can be seen in the following particular example: An arbitrary 14% increase in the differential cross-section data for Ne^+ on Ne taken at 25 kev was found to be sufficient to raise the corresponding $rV(r)$ curve in Fig. 4(c) until it was in line with the 50-kev curve. Such a scale factor error is well within possible experimental error. The fact that all curves seem to approach $Z_1Z_2e^2$ as r approaches zero shows that there is no gross error of this sort.

A second experimental difficulty is that scattered particle currents are extremely small and difficult to measure at large angles, especially in the light ion-atom combinations. There is much scatter in the data and this might possibly explain the diverse slopes and discontinuities of all the combinations of Fig. 5.

b. Extrapolation Errors

In Sec. 3(a) above an extrapolation was necessary because of the lack of differential cross section data beyond the largest angle measured. Besides the reasonable and smooth extrapolation used to extend the curve of Fig. 1(b), two extreme and less reasonable extrapolations were investigated.

(1) It was assumed that the differential cross section did not decrease below the last measured value and was constant out to 180°. Since $\sigma(\theta)$ is a decreasing function of angle, this grossly overestimates its value. When this assumption is followed through it causes the left end of the $rV(r)$ curves to turn up as shown for the 25-kev Ar^+ on Ar case in the curve labeled A in Fig. 4(a).

(2) The second assumption is that $\sigma(\theta)$ drops exponentially with angle as shown by the straight line labeled B on Fig. 1(a) joining smoothly to the data. Since the measured data have an upward curvature on this semi-log plot this assumption is somewhat of an underestimation of $\sigma(\theta)$ and the effect is to slightly lower the left end of the $rV(r)$ curves. This is shown for the 25-kev Ar^+ on Ar case by the curve labeled B in Fig. 4(a).

The other extrapolation, made necessary as discussed in Sec. 3(b) by the lack of data between 0° and 1°, was investigated in a similar manner, taking extreme assumptions and determining their effect on the final $rV(r)$ curves. These assumptions had only very small effects on the right end of these curves.

PHYSICAL REVIEW VOLUME 120, NUMBER 6 DECEMBER 15, 1960

Coulomb Energies of Closed-Shell Nuclei from Shell-Model Wave Functions*

N. V. V. J. Swamy and V. K. Kembhavi
Karnatak University, Dharwar, India

and

D. G. Galgali
Institute of Science, Bombay, India

(Received June 1, 1960; revised manuscript received August 11, 1960)

Using harmonic oscillator wave functions, the Slater integrals have been evaluated and expressed in the form of summation formulas. The Coulomb energies of seven closed-shell nuclei are estimated using these integrals. These estimates are compared with those based on a statistical model and a trapezoidal model. The influence of exchange energy on the Coulomb radius of a nucleus is shown to be sensitive to the model used. Although the $Z^{\frac{4}{3}}$ variation of exchange energy appears to be a suitable characterization, present estimates require a larger multiplying constant in the usually accepted expression for the exchange energy. The direct and "net" energies, computed from the three models, show very good agreement.

A STUDY has been made by Swamy and Green[1] of the Coulomb exchange energies of light nuclei, wherein it was noticed that estimates with shell-model wave functions do not agree with those of Bethe and Bacher[2] based on the statistical model of the nucleus. This study of Coulomb energies is now extended to heavier nuclei up to $Z=70$. In order, however, to facilitate a close comparison of the direct energies with the results of a uniform spherical distribution of charge, the present calculations are restricted to closed-shell nuclei. The Slater integrals[3] have been evaluated using harmonic oscillator wave functions and the results are given in the Appendix. The direct and exchange energies are linear functions of the oscillator parameter α. These, inclusive of self-energies, have been calculated for seven nuclei and are shown in Table I.

If a phase-shift analysis were made with the oscillator model to fit electron scattering, an exact experimental oscillator constant could have been available which would uniquely determine the nuclear radius. In our qualitative study we have, however, chosen the oscillator parameter to satisfy the "equivalent uniform radius" criterion

$$[5/3\ \langle r^2\rangle]^{\frac{1}{2}}=r_0A^{\frac{1}{3}}=R, \tag{1}$$

where $\langle r^2\rangle^{\frac{1}{2}}$ is the rms radius of the charge distribution computed with harmonic oscillator wave functions, and r_0 is the familiar radius constant. In the case of $_{20}Ca^{40}$ we have assumed r_0 to be equal to 1.22 in order to secure

* This work was supported by the Department of Atomic Energy, Government of India.

[1] N. V. V. J. Swamy and A. E. S. Green, Phys. Rev. **112**, 1719 (1958).

[2] H. A. Bethe and R. F. Bacher, Revs. Modern Phys. **8**, 162 (1936).

[3] E. U. Condon and G. H. Shortley, *The Theory of Atomic Spectra* (Cambridge University Press, Cambridge, 1951), p. 176.